The Astronomical Journal, 130:659–673, 2005 August

MODELS FOR INTERSTELLAR EXTINCTION IN THE GALAXY

E. B. Amôres[1,2] and J. R. D. Lépine[1]
Received 2004 February 25; accepted 2005 April 14

ABSTRACT

We present two models for the interstellar extinction in the Galaxy that are based on the hypothesis that the interstellar dust is well mixed with the gas, with a constant ratio (except for a small dependence of metallicity on the Galactic radius), and therefore that the extinction is proportional to the column density of the gas. In the first model we assume that the Galaxy is axisymmetric; the gas density in the disk is a function of the Galactic radius and of the distance perpendicular to the Galactic plane, and the extinction is proportional to the column density of the gas. In the second model we take into account the spiral structure of the Galaxy. In this case, instead of increasing almost linearly with distance, the extinction increases by steps each time a spiral arm is crossed, but only increases slowly in the interarm regions. The gas density distribution is obtained from the Berkeley and Parkes H I surveys and from the Columbia University CO survey. The *IRAS* 100 μm brightness distribution is also used as a tracer of the interstellar dust column density. The predictions of the models are compared with data taken from a number of catalogs that present color excess and distances for large samples of stars. Our models are useful for estimating distances of objects and color corrections for objects for which the distance can be estimated by some other method, and also for star counts and brightness models of the Galaxy, among other applications.

Key words: dust, extinction — Galaxy: structure — ISM: clouds — ISM: structure — stars: distances

1. INTRODUCTION

The ability to estimate interstellar extinction is essential for color corrections and distance calculations of all sorts of astronomical objects and is fundamental to Galactic structure studies. Many efforts have been made since the pioneer works of Trumpler (1930) and Parenago (1940) to describe the extinction in the Galaxy. Among others, Fitzgerald (1968) studied the distribution of interstellar reddening material within a few kiloparsecs of the Sun. Lucke (1978), Neckel & Klare (1980, hereafter NK80), and Perry & Johnson (1982) calculated extinctions for thousands of stars and derived diagrams of extinction versus distance. Burstein & Heiles (1978, 1982) presented reddening maps for high Galactic latitudes ($|b| \geq 10^{\circ}$), based on Galaxy counts and neutral hydrogen column densities. The works of Arenou et al. (1992) and Hakkila et al. (1997), based on different data, have in common the fact that they divide the sky into many areas, and their models are in practice a way of presenting previously tabulated results. Méndez & van Altena (1998, hereafter MvA98) presented a model that predicts reddening in the solar neighborhood. Schlegel et al. (1998, hereafter SFD98) constructed maps of far-infrared emission from dust using *IRAS* and DIRBE data. They calibrated the maps using the colors of elliptical galaxies to derive the reddening per unit flux density at 100 μm. That study provides the total dust emission in a given direction but not the extinction as a function of distance in the Galaxy. Moreover, Chen et al. (1999) performed extinction studies based on the SFD98 maps and found systematic errors in comparisons with stellar cluster data. They attributed part of the errors to the simplifications introduced by SFD98 in their model. These problems are further discussed in § 4.5.

Our purpose in this work is to present real models for the interstellar extinction in the Galaxy. What we call a real model is a model based on a description of the dust distribution in the whole Galactic disk, in contrast with series of maps or tabulated empirical measurements. Such a model must rely on our knowledge of the Galactic structure and must be able to predict extinctions to large distances in the Galactic plane. Of course, the difficulty in modeling the interstellar extinction comes mainly from the clumpy distribution of interstellar matter. One might think that since the dust distribution is clumpy, it should be safer to rely on empirical extinction maps than on any theoretical model. Therefore, a part of our task is to prove that in spite of its clumpy nature, the extinction is predictable, within errors that are acceptable for many purposes. As a by-product of the extensive comparisons with observational results that we make, we are able to provide the users of our models with an estimate of the probable error for a given observed object, which is obviously an important piece of information.

In the models presented in this work we calculate the interstellar extinction for any point in the Galaxy, given its Galactic coordinates (l, b) and distance. We constructed two models based on the distribution of gas (H I and CO) and interstellar dust (*IRAS* 100 μm). This was also the starting point of previous studies such as that of SFD98. We make use of the fact that gas and dust are well mixed, and therefore the extinction can be derived from the gas distribution. The proportionality between dust and gas column densities is well established. Among the first works that established this important result, Bohlin et al. (1978) found a good correlation between $N_{\rm H}$ and $E(B-V)$ for approximately 100 stars, some of them situated as distant as 3 kpc. More recently, Kim & Martin (1996) summarized the studies of the dust-to-gas ratio in the Galaxy. They combined the data obtained by different authors and found an excellent correlation between dust and gas. Xu et al. (1997) investigated the internal extinction and gas column density in spiral galaxies. They concluded that (1) the method for extinction correction based on the gas column density is a robust one, and (2) in the inner part of galaxy disks where most of the extinction occurs, the dust-to-gas ratio is on average about the same as the solar neighborhood value. They also concluded that most of the extinction is due to dust associated with molecular clouds.

[1] Instituto de Astronomia, Geofísica, e Ciências Atmosféricas da Universidade de São Paulo, Cidade Universitária, 05508-900 São Paulo, SP, Brazil; amores@astro.iag.usp.br.

[2] Observatoire de Besançon, 41 bis Avenue de l'Observatoire, B.P. 1615, 25010 Besançon Cedex, France.

The difference between our two models is that one is axisymmetric and the other takes into account the spiral structure. In model A the Galaxy is assumed to have axial symmetry, with the gas density varying radially in a smooth way, so that the interstellar extinction integrated along a line of sight also varies smoothly. In model S (with spiral arms) the extinction, instead of growing almost linearly with distance, increases by large steps each time a spiral arm is crossed and stays almost at the same level in the interarm regions. This behavior is observed in the diagrams of extinction versus distance in some directions (NK80; Fitzgerald 1968). The distance from the Sun to the Galactic center used in our models is 7.5 kpc, as suggested by Reid (1993), but the results can be easily scaled to other choices of R_0.

In § 2 we list the H I, CO, and infrared data surveys used for the construction of the models. The corrections that are needed to transform the infrared observations into column densities are discussed. The descriptions of the two extinction models and a comparison between their predictions are given in § 3. The predictions of the two models are compared in § 4 with the observed extinctions from a number of catalogs that present distances and extinction or color excess for large samples of stars. Comparisons with the SFD98 and Burstein & Heiles (1978, 1982) maps are also presented.

2. OBSERVATIONAL DATA ON GAS DISTRIBUTION

The H I data were obtained from the Berkeley survey (Weaver & Williams 1973), which covered the strip of Galactic longitude $10^\circ \leq l \leq 250^\circ$, from the Parkes survey (Kerr et al. 1986), which covered $240^\circ \leq l \leq 350^\circ$, and from the NRAO survey (Burton & Liszt 1983, hereafter BL83), which covered $349^\circ \leq l \leq 13^\circ$ for the region of the Galactic center. All these surveys covered Galactic latitudes less than 10°.

The antenna temperatures of the Parkes survey were multiplied by a factor of 1.14 to get a uniform calibration with the Berkeley survey. This factor was obtained by analyzing the overlapping region (Amôres 2000). The antenna temperatures of the NRAO survey were calibrated with the Berkeley survey using the relation given by BL83. The CO data were obtained from the Columbia survey (Dame et al. 1987, 2001).

To describe the dust distribution in the Galaxy we used the *IRAS* data (Hauser et al. 1984) in the bands at 12, 25, 60, and 100 μm. We applied a blackbody brightness temperature correction to the 100 μm band as described below.

2.1. *Corrections to the* 100 μm *Flux*

The emission at 100 μm is optically thin throughout the Galaxy, which makes it ideal for estimating the quantity of dust along a line of sight without worrying about self-absorption. The brightness of the Galaxy at 100 μm is dominated by the thermal emission of large dust grains that are in radiative equilibrium in the interstellar medium. In the literature, grain temperature estimates are in the range 18–28 K. Bloemen et al. (1990), based on the 60 μm–100 μm color index, found dust temperatures of about 24 K for dust mixed with atomic gas and about 22 K for dust in molecular clouds. They also found that in regions close to OB stars or H II regions, the equilibrium temperature reaches higher values. Temperatures around 18–19 K are mentioned in several papers (Laureijs et al. 1991; Lee & Draine 1985; Terebey & Fich 1986). As pointed by Boulanger et al. (1998), the discrepancies can be explained by assuming the presence of an additional emission component at 60 μm (see the review by Cox & Mezger 1989). In principle, the far-infrared emission is not merely proportional to the column density of dust, since it depends on the temperature, but the effect of varying temperature can be taken into account, since the temperature can be estimated by means of the ratio of intensities between 60 and 100 μm.

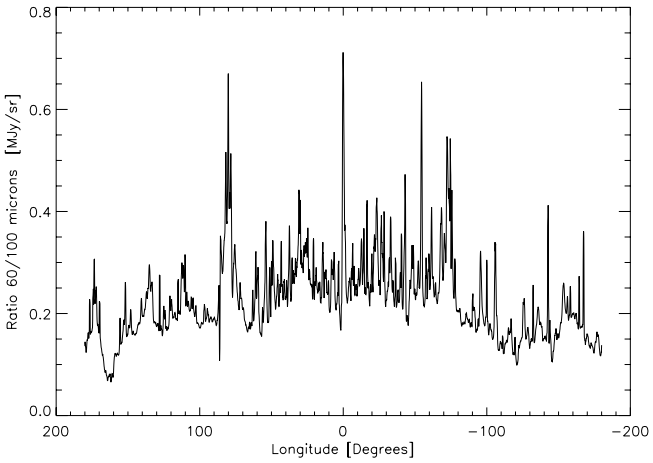

FIG. 1.—Longitudinal profile of the ratio between the flux densities at 60 and 100 μm.

The ratio between intensities at 60 and 100 μm is shown in Figure 1 as a function of Galactic longitude, in the Galactic plane ($b = 0^\circ$); the peaks correspond to larger temperatures, usually found in the spiral arms. It can be seen that this ratio does not present large variations; in particular, it does not show any significant increase in directions close to the Galactic center. The mean ratio is $\simeq$0.20, which corresponds to a temperature of 23 K if it is assumed that the optical depth varies as $\lambda^{-1.5}$.

The constancy of the ratio $I_{60\ \mu\mathrm{m}}/I_{100\ \mu\mathrm{m}}$ does not necessarily imply uniformity of the interstellar radiation field. This ratio can be influenced by the nonthermal balance of the small grains, which contribute a large part to the emission at 60 μm.

From Planck's law and supposing that the emissivity of the dust grains varies as $\lambda^{-1.5}$, we conclude that the temperature (in kelvins) can be approximated by

$$T = 15.1 + 300\,\frac{I(60\ \mu\mathrm{m})}{I(100\ \mu\mathrm{m})} - 1341\left[\frac{I(60\ \mu\mathrm{m})}{I(100\ \mu\mathrm{m})}\right]^2, \quad (1)$$

where I is the flux in MJy sr^{-1}. Knowing the temperature from this relation, we calculate the ratio of the 100 μm intensity from the grains at temperature T to the intensity that would be observed if the grains were at a standard temperature, e.g., 23 K. In this way we obtain the correction factor f_c to be applied to the observed intensity in order to have a dust column density proportional to the intensity. The precise value of the standard temperature is not important; what is important is to normalize the emission of different directions to the same temperature.

The dependence of f_c on temperature, for a standard temperature of 23 K, is well fitted by the polynomial

$$f_c = 2.11 - 0.151T - 0.00541T^2 + 4.3\times10^{-4}T^3, \quad (2)$$

where f_c is such that

$$F_c(100\ \mu\mathrm{m}) = F(100\ \mu\mathrm{m})/f_c. \quad (3)$$

The equation above is valid for $T \geq 15$ K, i.e., $I_{60\ \mu\mathrm{m}}/I_{100\ \mu\mathrm{m}} \geq 0.07$. Of course, the correction that we are proposing is only an approximation, or an "average" correction, since the temperature

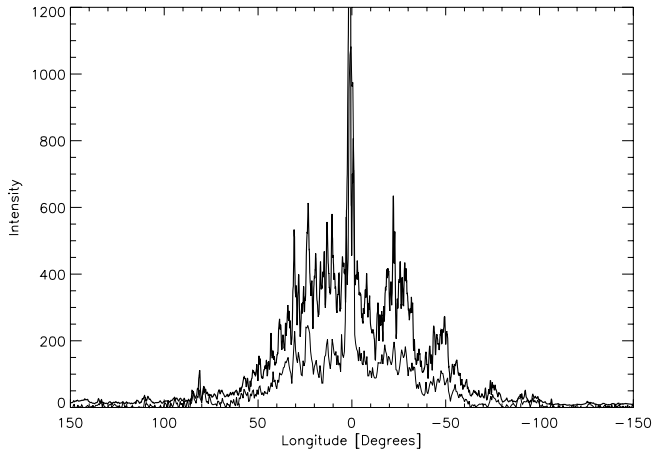

FIG. 2.—Corrected flux density at 100 μm (*thick line*) and integrated intensity of CO (*thin line*), in arbitrary units as functions of Galactic longitude.

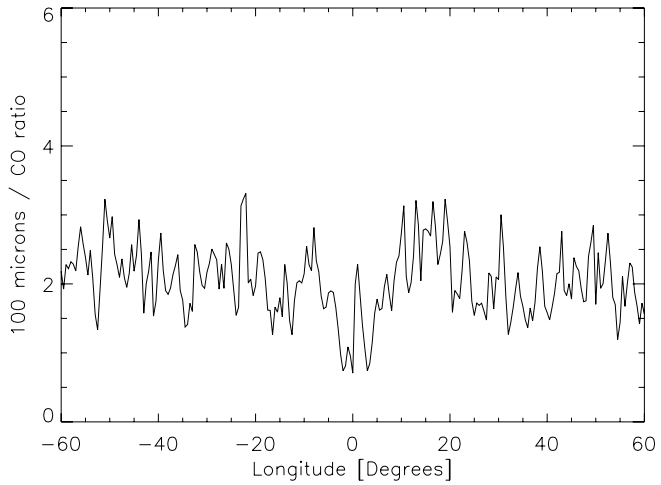

FIG. 3.—Ratio of corrected 100 μm flux to integrated CO emission, in arbitrary units as a function of Galactic longitude.

of the dust may vary along the line of sight. The longitudinal profile of the corrected intensity at 100 μm in the Galactic plane ($b = 0^\circ$) is shown in Figure 2; the figure also shows the longitudinal profile of the integrated intensity of CO. The similarity of the two curves is remarkable; a scaling factor can make them almost coincide. The ratio between corrected 100 μm flux and integrated CO intensity is shown in Figure 3 for the longitude interval $-60^\circ \leq l \leq 60^\circ$. Outside this interval, the atomic gas starts to dominate, and there are regions with almost no CO (see § 3).

The good correlation between CO and corrected 100 μm highlights important points for the present work: (1) the dust and gas are well mixed and are observed with a constant proportion in all directions; (2) the corrected 100 μm flux can be considered as a good indicator of the column density of dust; and (3) the dust and CO are concentrated in the inner parts of the Galaxy ($|l| \leq 60^\circ$) and present peaks related to the tangential directions of the spiral arms.

The fact that molecular clouds and CO emission are relevant tracers of the spiral structure is a consequence of the presence of interstellar shocks in the arms, which produce an increase of the gas density and transform H I into H_2 (see, e.g., Marinho & Lépine [2000] for the chemistry involved). The molecular clouds are short lived and return to the form of H I gas in the interarm region.

3. MODELS OF GAS DISTRIBUTION

The procedure adopted to calculate the interstellar extinction assumes that the extinction is proportional to the column density of hydrogen in both its atomic and molecular forms:

$$A_V = \gamma(R) N_{\rm H\,I}(r,\ z) + 2\gamma(R) N_{\rm H_2}(r,\ z), \qquad (4)$$

where $N_{\rm H\,I}$ and $N_{\rm H_2}$ are the column densities and γ is a factor of proportionality. An average value $\gamma = 5.3 \times 10^{-22}$ mag cm^2 was estimated by Bohlin et al. (1978). A similar equation holds for $E(B - V)$; the ratio between total and selective extinction is taken to be 3.05 (Whittet 1992). Because of the well-known metallicity gradient in the Galactic disk, it is expected that the amount of dust per unit gas column density will vary, so that γ in equation (4) decreases with R. Based on observations of the Galactic disk and of external galaxies we use a law such as $R^{-0.5}$, which is valid for galactocentric radii $R > 1.2$ kpc. For smaller R, the metallicity is highly uncertain, and a constant value is used. The correction for metallicity is only applied to hydrogen in the atomic phase; the molecular hydrogen has its density traced by CO, which is already affected by metallicity effects and does not need any further correction. Equation (4) is written in a simple form for clarity; in practice, for the first term, since γ depends on R one has to integrate the gas density along the line of sight multiplied by the local value of γ. Another point concerning equation (4) is that the factor in the second term can be different from 2, since the grains in molecular clouds may have a different composition from those in atomic gas; for instance, they may have hydrogen-rich mantles. We later propose small adjustments of the constants.

3.1. *The Radial Gas Density Distribution: Axisymmetric Model*

The radial distributions of the two gas densities (in units of cm^{-3}) needed to compute column densities in equation (4) were derived from the H I and CO surveys mentioned in § 2. Analytical expressions were derived for the two radial density distributions, using the same procedure. At intervals of 1° and for the entire range of longitudes, we compared the "observed" column density, obtained by integrating the spectra over velocity, with the "theoretical" column density, obtained by integration of a tentative radial density function along lines of sight crossing the whole Galaxy. The rms difference was minimized by varying the parameters of the analytical expression (Fig. 4). The constant used to transform the integrated intensity of CO to column density of H_2 was 1.8×10^{20} cm^{-2} (K km s^{-1})$^{-1}$ (Dame et al. 2001). For H I, 1 K km s^{-1} corresponds to a column density of 1.8×10^{18} H I molecules cm^{-2}. After a number of experiments, we adopted similar analytical expressions for both gas phases:

$$n_{\rm H\,I,\ H_2} = c \exp\left[-\frac{r}{a} - \left(\frac{b}{r}\right)^2\right], \qquad (5)$$

with the adjusted parameters a, b, and c presented in Table 1. The H I and H_2 density distributions as functions of galactocentric radius are shown in Figure 5. The large concentration of H_2 in the Galactic center (for $r < 1.2$ kpc) was adjusted separately with the function $n_{\rm H_2} = \beta \exp\left[-(r/\alpha)^2\right]$, with the constants $\alpha = 0.1$ kpc and $\beta = 240.0$ cm^{-3}.

3.2. *The Density Distribution Perpendicular to the Galactic Plane*

The vertical distribution of the gas in atomic and molecular form is described by a Gaussian function of z. This distribution is

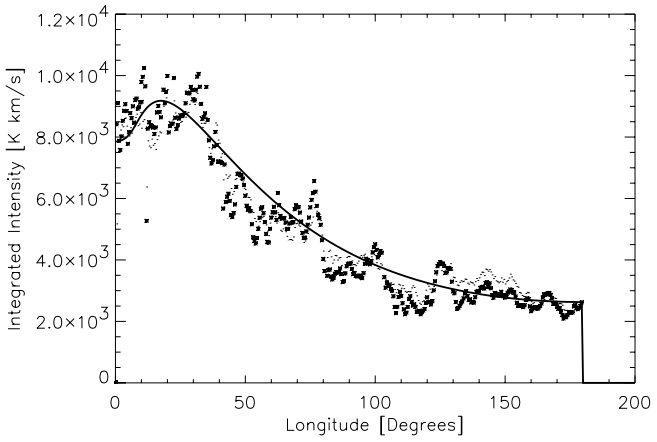

FIG. 4*a*

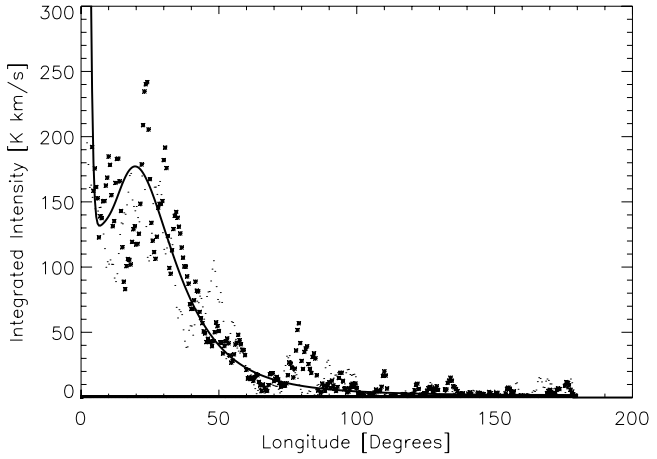

FIG. 4*b*

FIG. 4.—Theoretical vs. observed longitudinal profiles of integrated intensity for (*a*) atomic hydrogen and (*b*) molecular hydrogen. We make use of axisymmetry and plot on the same axis l and $360^\circ - l$ for $l < 180^\circ$ (*asterisks*) and $l > 180^\circ$ (*dots*), where solid lines show fitted curves.

expected from simple hydrostatic equilibrium considerations in the case in which gravity increases linearly with $|z|$, a good approximation for $|z|$ smaller than about 200 pc. Furthermore, the Gaussian distribution is found to correctly fit the observations. Because of a number of deviations of the gas distribution with respect to the Galactic plane, the Gaussian is not always centered on $z = 0$ but on z_c:

$$n_{\rm H}(r,\ z) = n_{\rm H}(r,\ z_c) \exp\left[-\left(\frac{z - z_c}{1.2 z_{1/2}}\right)^2\right]. \qquad (6)$$

The scale height $z_{1/2}$ (half-width at half-maximum) grows exponentially with r, a result obtained for CO by Sanders et al.

TABLE 1
PARAMETERS OF THE RADIAL DENSITY FUNCTIONS FOR H I AND H_2

Species	*a* (kpc)	*b* (kpc)	*c* (cm^{-3})
H I	7.0	1.9	0.7
H_2	1.2	3.5	58.0

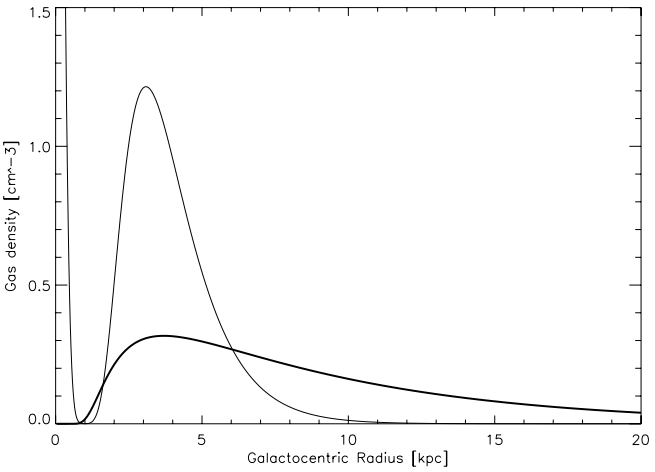

FIG. 5.—Distribution of gas density (cm^{-3}) in the Galactic plane as a function of galactocentric radius (kpc) for H I (*thick line*) and H_2 (*thin line*).

(1984) and Bronfman et al. (2000) and confirmed by E. B. Amôres & J. R. D. Lépine (2005, in preparation, hereafter Paper II).

The CO data can be fitted by

$$z_{1/2} = 45 \exp(0.10r), \qquad (7)$$

in which $z_{1/2}$ is given in parsecs and r in kiloparsecs. The scale height for H I was described by Guibert et al. (1978); it follows a radial variation similar to that of CO, with a similar scale length. The H I scale height can be obtained by multiplying that of CO by a factor of 1.8. Note that the increase of the scale height as a function of Galactic radius is expected from the fact that the stellar density, and consequently also the gravity in the z-direction, decreases with r. The difference between the scale heights of H I and H_2 is related to the difference in average temperature of atomic and molecular gas.

The zero height z_c is a parameter useful for describing the corrugation of the Galactic plane, the warp at large distances, and the fact that the Sun is not situated exactly in the middle of the Galactic disk in the z-direction. In the present work, we only took into consideration the displacement of the Sun, which is supposed to be 20 pc above the middle of the gas distribution ($z_c = -20$ pc; Hammersley et al. 1995).

3.3. *A Model of Gas Distribution with Spiral Arms*

In the first model (A) described above we assumed an axisymmetric gas distribution, in which the gas density in the disk is a function of only the galactocentric radius and the distance to the Galactic plane. In the second model (S) we take into account the spiral structure of the Galaxy. The major difficulty that we have to face is that like other spiral galaxies, our Galaxy has a complex structure, with arms that present changes in pitch angle, bifurcations, spurs, etc. There is not yet in the literature a fully accepted model of the spiral structure with a corresponding mathematical description of the arms. Theoretical and observational justifications for a model with two+four arms, in which the two arms and four arms have different pitch angles, are discussed by Lépine et al. (2001), while Vallée (2002) and Russeil (2003) argue in favor of a four-arm structure. However, none of these descriptions account for details of the observed structure, such as changes in the direction of the arms, that are not fitted by logarithmic spirals.

Our choice in the present paper is to adopt an empirical model of the spiral structure based on the analysis of the distribution of

TABLE 2
MAIN PARAMETERS OF THE SPIRAL ARMS TRACED BY MOLECULAR HYDROGEN (DUST) USED IN THE SPIRAL MODEL

Arm	Tangential Directions (deg)	Pitch Angle (deg)	Initial Radius (kpc)	Initial Phase (deg)	Arm Extension (deg)	Peak Density (cm^{-3})	Width (kpc)
1	32.07/−52.6	12.3	2.40	165.0	360	2.05	0.14
2	49.0/−26.1	7.0	2.70	340.0	380	0.1	0.13
3	−70.0	13.8	6.50	353.0	120	6.0	0.08
4	−34.2	13.5	3.65	30.0	150	10.0	0.14
5	−21.4	7.5	2.50	20.0	345	0.50	0.06
6	24.1/−44.7	11.7	2.90	285.0	180	1.00	0.08
7	71.0/−88.0	6.0	6.80	330.0	80	24.0	0.04
8		10.1	7.10	240.0	140	0.8	0.13
9		7.0	8.40	220.0	140	2.0	0.13
10		8.0	7.50	330.0	40	4.0	0.08
11	−57.13	10.0	7.90	290.0	130	10.0	0.15
12		10.0	5.70	5.0	150	1.25	0.14
13		55.0	5.10	345.0	15	10.0	0.13
14	41.1	6.2	6.50	185.0	110	30.0	0.13

many tracers, such as H II regions, H I, and CO, and on the tangential directions given by the *IRAS* 100 μm brightness distribution and the *COBE* DIRBE data. The construction of such a model of the spiral structure is a complex task, the description of which is outside the scope of this work and will be presented in a separate paper (Paper II). As the distribution of the molecular and atomic hydrogen are different, it was necessary to adjust the spiral arms of H I and the spiral arms traced by CO separately. A result of this study is that there is a significant contribution of H I in the interarm regions (model A is a good description of the H I distribution). In contrast, the molecular gas is strongly concentrated in the arms, with almost no H_2 in the interarm regions, so that model S is a clearly better description of this component.

A large number of parameters is required to describe the two complex spiral structures, which are slightly different. The number of parameters may seem excessive for a model aimed to reproduce the extinction in the Galaxy. However, a simplified model would not be realistic. Many arm segments with different pitch angles are needed because real arms are not well represented by a single logarithmic spiral that follows a long path around the Galaxy. In addition, there are bifurcations and some short bridges. We remark, however, that the positions of the spiral arms were not adjusted to give the best results in the comparison of calculated versus observed extinction. In this sense, the structure is external to the extinction model, like the parameters that describe the gas density distribution in the axisymmetric model. The parameters express what we believe to be the best model of gas distribution as derived from different types of observations. If a better description of the spiral structure of the Galaxy becomes available, we can easily substitute for the present one. For the moment, the important point is to verify whether the presence of a spiral structure is relevant for calculations of extinction.

The arms or segments of arms are considered as Gaussian distributions of gas density in the radial direction, centered on the radius r_a of the arm and given by the spiral equation

$$r_a = r_0 \exp[(\theta - \theta_0) \tan i], \quad (8)$$

where r_0 and θ_0 are the polar coordinates of the starting point of the arm and i is the inclination of the arm. Therefore, four parameters are used to describe the geometry of an arm: r_0, θ_0, i, and $\Delta\theta$ (total extension of the arm), and two parameters describe the "intensity" of the arm: the peak density and width of the Gaussian. The parameter that we call "extension" of the arms is the angle between the extremities of the arms as seen from the Galactic center. Actually, the peak value of the Gaussian that gives the profile of an arm is not directly the density but a factor that multiplies the underlying average or axisymmetric gas density (H I or H_2). In other words, the peak values of density in the H_2 and H I arms have the same radial variation as model A (eq. [5] with the constants in Table 1); the relative enhancement of density is assumed to be constant along a given arm. The scale height of the arms is also the same as in the model without arms (model A).

We give in Tables 2 and 3 the complete list of spiral arms included in the empirical model and show in Figures 6*a* and 6*b* that these arms fit correctly the longitude-velocity diagrams. The face-on aspect of the adopted structures is shown in Figures 6*c* and 6*d*. Table 2 gives the parameters of the molecular hydrogen spiral arms; these arms fit the *l*-*v* diagram of H II regions in the Galaxy (Paper II). It is known that the H II regions are normally associated with molecular clouds, so that we can use the H II regions as tracers of molecular arms. The H II regions shown in the *l*-*v* diagram (Fig. 6*a*) were taken from the catalog of Russeil (2003). For H I (Fig. 6*b*) the points represent the maxima of intensity observed in the spectrum of each direction, obtained from an analysis of the H I data.

While the position and extension of the arms come from the fitting of *l*-*v*, the Gaussian "intensity" parameters (width and peak density factor) were adjusted so as to fit the peaks seen in the longitudinal profile of interstellar dust (Fig. 7*a*) and integrated intensity of H I (Fig. 7*b*). The tangential directions to the arms, listed in Tables 2 and 3, are not independent parameters; they are derived from the equations of the arms. The tangential directions are in good agreement with the longitudes of the peaks of the 100 μm emission and H I integrated intensity, respectively. The tangential directions at 100 μm are the same as observed with different tracers (e.g., Englmaier & Gerhard 1999).

Figure 8 compares the behavior of the extinction with distance given by the two models (A and S), at 0° latitude for five different longitudes, and in one case also at latitude −4°, in order to illustrate that the models also vary correctly with latitude. The stars from the NK80 catalog situated within a small angle from the directions are plotted. It can be seen that in the spiral model the extinction grows by steps, with a strong increase in the extinction each time a spiral arm is crossed.

Although there are local differences between models A and S, there is no large excess extinction of one model with respect to

TABLE 3

MAIN PARAMETERS OF THE SPIRAL ARMS (BRIDGES, SEGMENTS, AND BIFURCATIONS) TRACED BY NEUTRAL HYDROGEN USED IN THE SPIRAL MODEL

Arm	Tangential Directions (deg)	Pitch Angle (deg)	Initial Radius (kpc)	Initial Phase (deg)	Arm Extension (deg)	Peak Density (cm^{-3})	Width (kpc)
1.....	−22.0	6.5	2.35	329.0	240	0.1	0.20
2.....	39.56/−50.62	6.7	3.80	195.0	330	0.3	0.13
3.....	30.0	7.1	2.57	155.0	200	0.1	0.15
4.....	−40.0	7.5	3.80	346.0	245	0.2	0.18
5.....	−63.0	6.4	7.50	357.5	182	1.3	0.13
6.....	−39.0	7.5	7.65	163.0	159	1.0	0.18
7.....	75.0/−84.0	5.3	5.90	222.0	279	0.3	0.25
8.....	−70.00	−22.0	9.05	345.0	24	4.0	0.14
9.....	75.0	11.6	6.44	225.0	110	1.1	0.22
10.....	−100.0/90.0	7.8	7.36	351.4	199	2.5	0.18
11.....	53.30	9.4	3.95	190.0	170	0.2	0.18
12.....		10.5	8.60	45.4	69	0.5	0.21
13.....		12.0	7.30	330.0	31	8.0	0.25
14.....	96.79	−40.0	11.40	315.0	31	2.0	0.14
15.....		11.1	10.10	350.0	48	2.0	0.19
16.....	80.0	9.0	5.00	315.0	25	3.0	0.19
17.....	−70.0	11.1	11.10	322.0	65	1.0	0.19
18.....		10.5	8.60	25.4	89	1.0	0.28

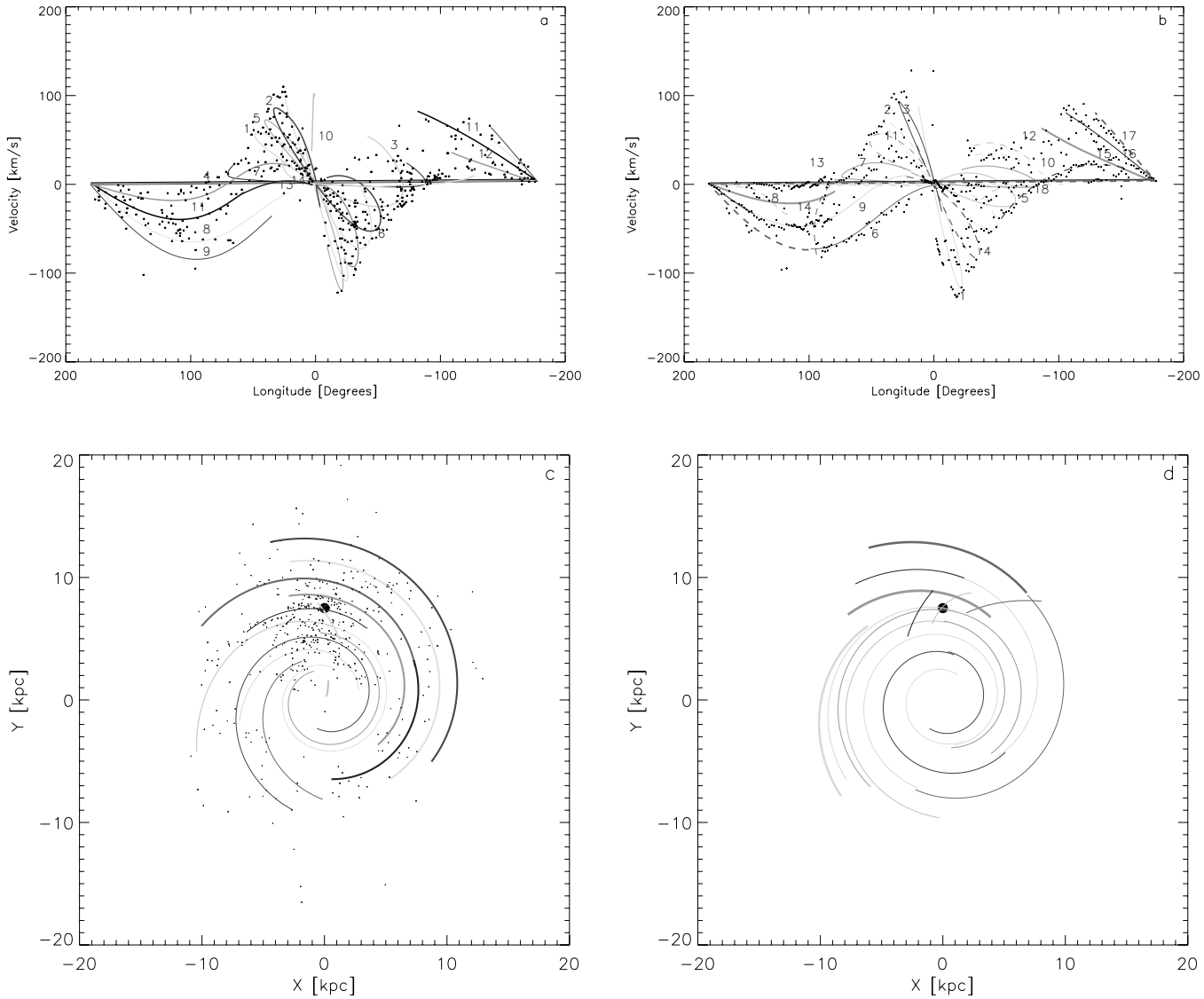

FIG. 6.—*Top*: *l*-*v* diagrams for (*a*) H II regions and (*b*) H I. *Bottom*: Face-on (*c*) H II regions and (*d*) H I. The lines represent the spiral arms, and the points are described in the text. The parameters of the arms are given in Tables 2 and 3.

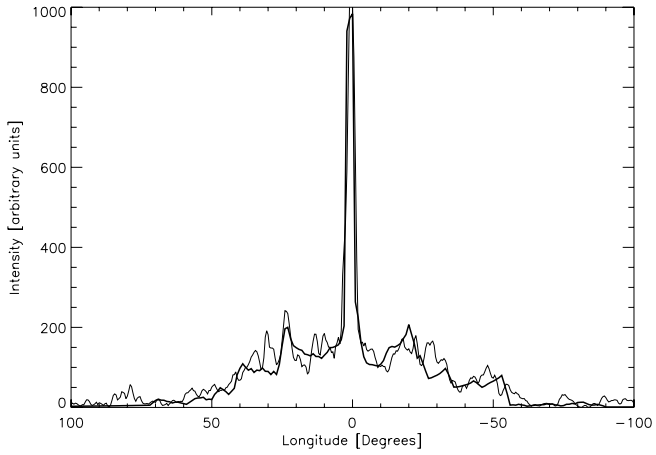

FIG. 7*a*

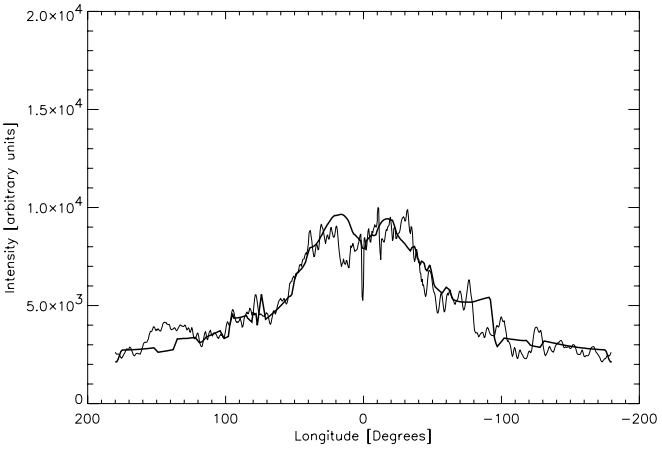

FIG. 7*b*

FIG. 7.—Longitudinal profiles of (*a*) corrected intensity at 100 μm (*thin line*) and the spiral model fit of molecular hydrogen distribution (*thick line*), and (*b*) integrated intensity of H I (*thin line*) and the spiral model fit to neutral hydrogen (*thick line*).

the other, as can be seen from their longitude-averaged extinction (Fig. 9). To construct these curves, for each step of 50 pc in distance in the Galactic plane (latitude 0°), the extinction was averaged over a solar circle, using intervals of 20° in longitude. The 1 kpc circle gives an average A_V of 0.96 mag kpc^{-1} for model A and 0.74 mag kpc^{-1} for model S. These values of extinction are in good agreement with those widely accepted in the literature. Note, however, that A_V for 1 kpc is much larger (about 50%) in directions close to the Galactic center than close to the anticenter, so that the average value is not very useful for comparisons.

4. MODELS VERSUS OBSERVATIONAL DATA

4.1. *Fine Tuning of the Parameters*

In the following we compare the prediction of the models with the data from catalogs of stars with measured extinction and distance. Since the catalog of NK80 is the most complete one, we also used it to minimize the errors by adjusting the factor γ of equation (4). This normalization with direct extinction measurements is supposed to cancel part of the errors that might have accumulated in the construction of the models, such as the calibration errors of the gas surveys. We adopted for both models $\gamma = 5.7 \times 10^{-22}$, which gives histograms of the calculated − observed $E(B - V)$ centered on zero magnitude. This is within the range of values of γ cited by Bohlin et al. (1978) and mentioned in § 3.

We remarked, based on the examination of the error maps and on a number of trials, that the extinction computed by model A in the longitude range 120°–200° had to be multiplied by about a factor of 2 in order to better match the stellar data. In other words, the Galactic disk presents some systematic deviations with respect to an axisymmetric model.

In model S this effect should not be important, since the arms are not axisymmetric anyway, and the individual adjustment of arm intensities already takes care of extinction differences in different directions. However, we remarked that the nearest arm observed in the first and fourth quadrant has its intensity decreased by a factor of 3 between longitudes 0° and 14°. In the comparisons next discussed, both models already include these respective longitude-limited corrections.

4.2. *The Neckel & Klare (1980) Catalog*

The catalog of extinction data of 12,547 O–F stars, Galactic clusters, and δ Cephei stars by NK80 presents spectral types derived from spectroscopy, equivalent widths of the Hβ line, and *UBV* data obtained from the literature and/or by the authors. The derived values of extinction and distances are also given.

The catalog contains 7565 stars of OB spectral type that are well distributed in Galactic longitude and latitude. Because of the large fraction of early-type stars, approximately 70% of the objects are located close to the Galactic plane (latitudes less than 10°). Half of the objects in the catalog are closer than 0.5 kpc; however, there is a reasonable amount of objects at larger distances, i.e., between 5 and 15 kpc, which are important for testing our extinction models, which are intended to describe the whole Galaxy.

4.2.1. *Model A*

Using model A we calculated the extinction for each star of the NK80 catalog from its longitude, latitude, and distance. The results were compared with the color excess given in the catalog. The rms difference $\delta E(B - V)$ (calculated − observed) was 0.25. This calculation excluded stars with absolute values of $\delta E(B - V)$ larger than 3 times the rms difference, approximately 2% of the original sample. Figure 10 shows $\delta E(B - V)$ as a function of longitude.

Approximately 7700 stars or 60% of the sample have absolute values of $\delta E(B - V)$ less than 0.15 mag. In Figure 10 a number of strips appear with stars with negative $\delta E(B - V)$, reaching about −0.5 mag; this can be attributed to the presence of dense clouds in these directions. The region situated in the range $100° < l < 140°$ is not very satisfactorily described by the model. Interestingly, MvA98 also found similar difficulties in this region (see their Figs. 4*a* and 8*a*). We do not know the origin of the discrepancies. They could be due to the warp of the Galaxy or to some other type of deformation of the plane. One can see in the distribution of regions of massive star formation (Bronfman et al. 2000) that in this range of longitudes, the sources are shifted in a systematic way from the plane, up to 2° in latitude.

In Figure 11 we present maps of calculated − observed $\delta E(B - V)$ in Galactic coordinates for three ranges of distances. These are not extinction maps but error maps. The purpose of the figure is to point out the regions of the sky where the quality of the model is satisfactory or not so good. Although the NK80 catalog contains a large sample of stars, some regions are devoid of stars, and the map was filled by the nearest $\delta E(B - V)$. An expected characteristic of the distribution of stars in this catalog is that in the first range of distance, they are distributed over the

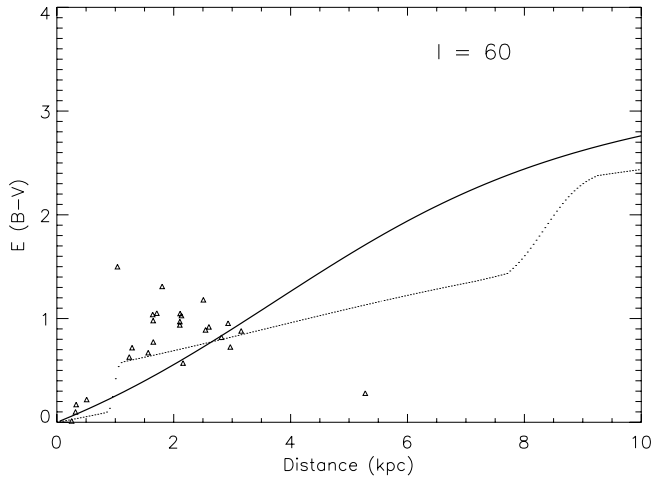

FIG. 8*a*

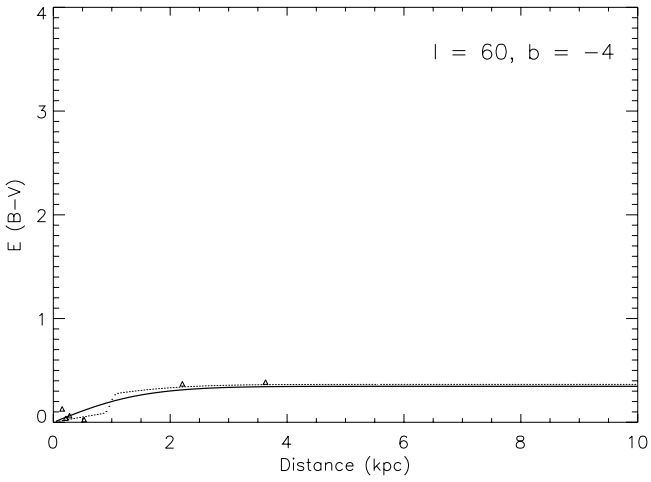

FIG. 8*b*

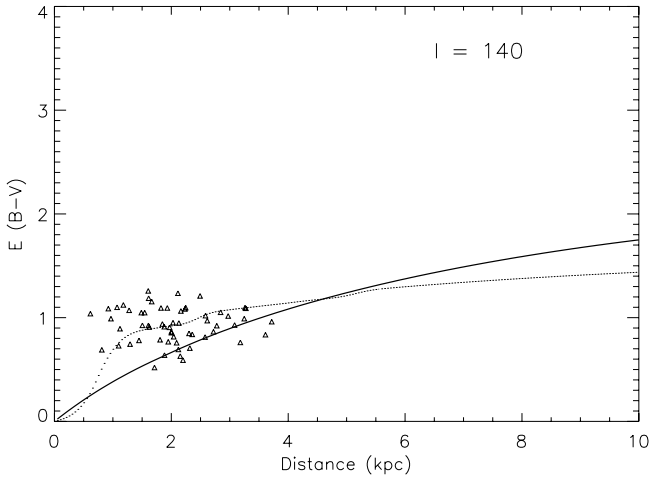

FIG. 8*c*

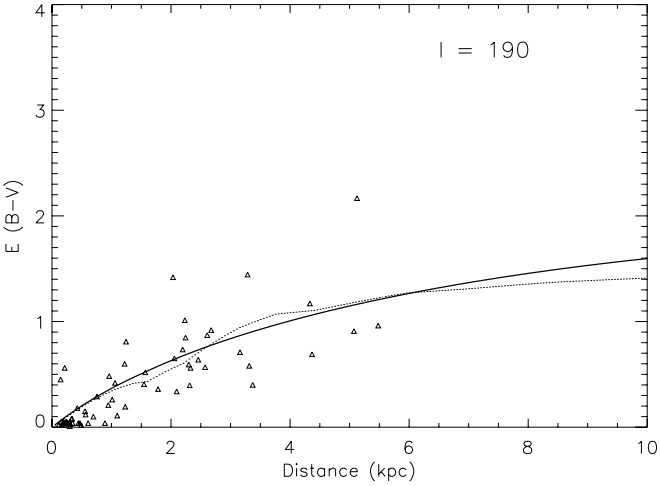

FIG. 8*d*

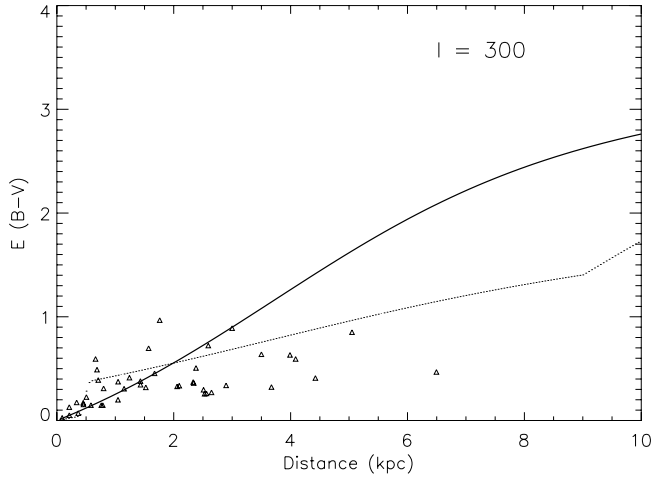

FIG. 8*e*

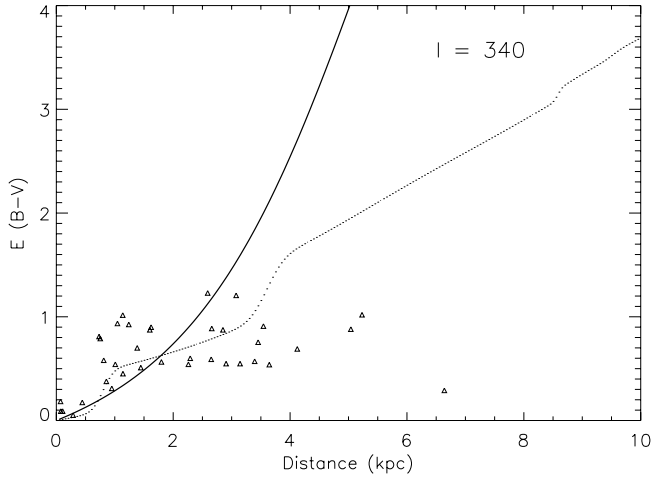

FIG. 8*f*

FIG. 8.—Extinction vs. distance, comparing model A (*thick lines*) with model S (*thin lines*). The plots are for latitude $b = 0^\circ$ except for panel *b* ($b = -4^\circ$); longitudes are (*a*) $l = 60^\circ$, (*b*) $l = 60^\circ$, (*c*) $l = 140^\circ$, (*d*) $l = 190^\circ$, (*e*) $l = 300^\circ$, and (*f*) $l = 340^\circ$. The stars from the NK80 catalog located within small angular distances of the directions given above ($\pm 3^\circ$ in longitude, $\pm 1^\circ$ in latitude) are shown.

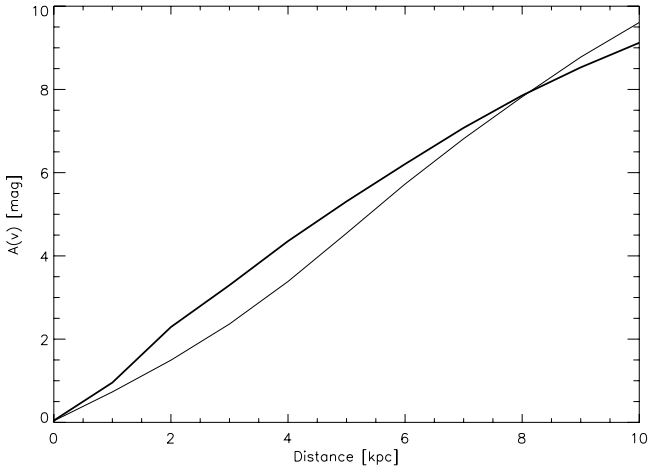

FIG. 9.—Extinction in the Galactic plane as a function of distance to the Sun, averaged over longitude for model S (*thick line*) and model A (*thin line*).

whole sky; more distant stars are concentrated at low Galactic latitudes.

Figure 12 shows the histogram of $\delta E(B-V)$ for stars of the NK80 catalog, for the same ranges of distance as in Figure 11. There are 5600 stars with $d \leq 1$ kpc, 3632 stars with 1 kpc $< d \leq 3$ kpc, and 1429 stars with $d > 3$ kpc. The width of the distribution grows with distance; in the first range of distance it is 0.05 mag, in the second 0.25 mag, and in the third 0.31 mag (σ from a Gaussian fit). These numbers can be considered as the typical uncertainties of the model. The Pearson's correlation coefficient (Babu & Feigelson 1996), hereafter denoted r, is 0.73 between the calculated and observed $E(B-V)$ for model A.

4.2.2. *Model S*

The results of model S were compared in a similar way with the extinction values of the NK80 catalog; the rms $\delta E(B-V)$ was 0.26, excluding the stars with absolute value greater than 3 times the rms. Figure 13 shows $\delta E(B-V)$ as a function of longitude.

Figure 14 presents the maps of $\delta E(B-V)$ for the stars of the NK80 catalog using model S, Figure 13 gives the $\delta E(B-V)$ distribution as a function of longitude, and Figure 15 gives the histograms for different ranges of distances. Like in the maps for model A, large regions with the same $\delta E(B-V)$, due to the lack of stars, can be seen in Figure 14. The Gaussian parameters σ in Figure 15 are slightly larger than for model A; for the first range of distance it is 0.06 mag, for the second 0.26 mag, and for the third 0.28 mag. The Pearson's correlation coefficient r is 0.72 for model S.

It is important to note that the difference between the calculated and observed $E(B-V)$ should not be attributed to the models only but is partly explained by the intrinsic errors of the stellar data.

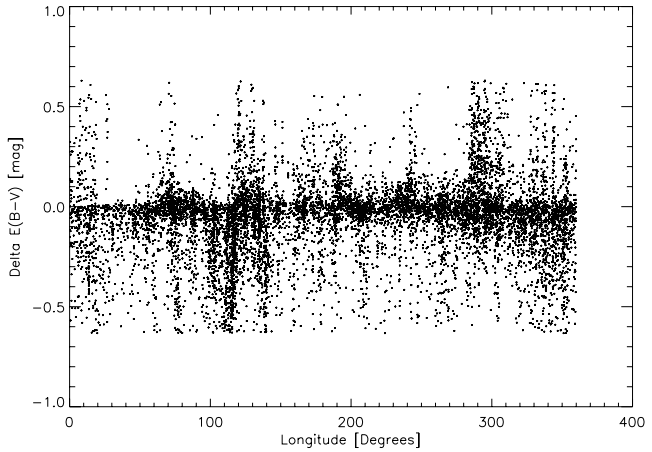

FIG. 10.—Difference between calculated and observed color excess $\delta E(B-V)$ for stars of the NK80 catalog using model A, as a function of Galactic longitude.

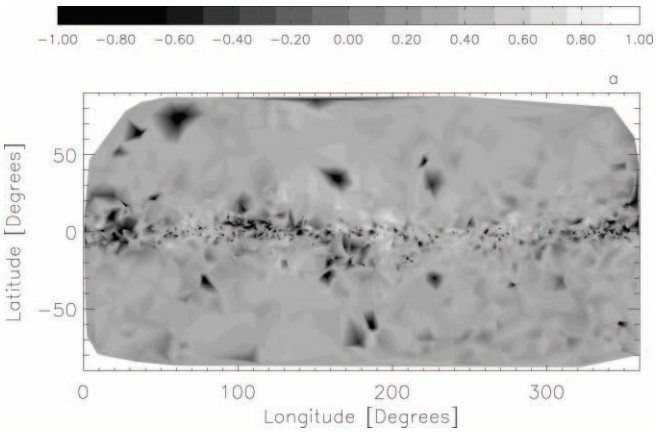

FIG. 11*a*

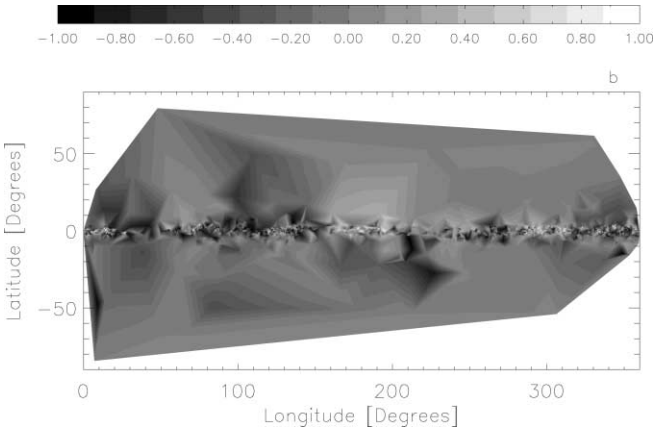

FIG. 11*b*

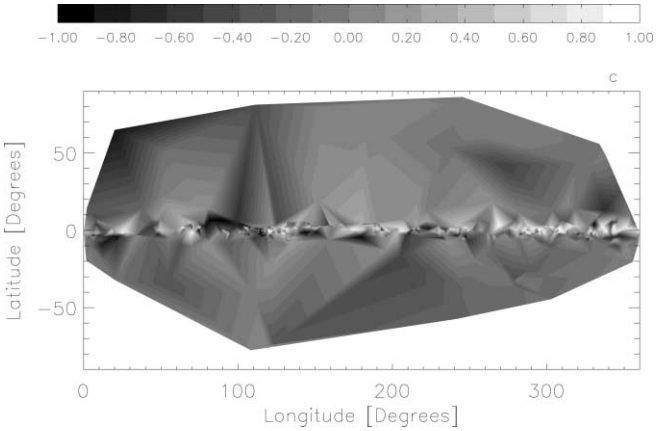

FIG. 11*c*

FIG. 11.—Maps of errors $\delta E(B-V)$ for stars of the NK80 catalog using model A in three ranges of distances d: (*a*) $d \leq 1$ kpc, (*b*) 1.0 kpc $< d \leq 3.0$ kpc, and (*c*) $d > 3.0$ kpc.

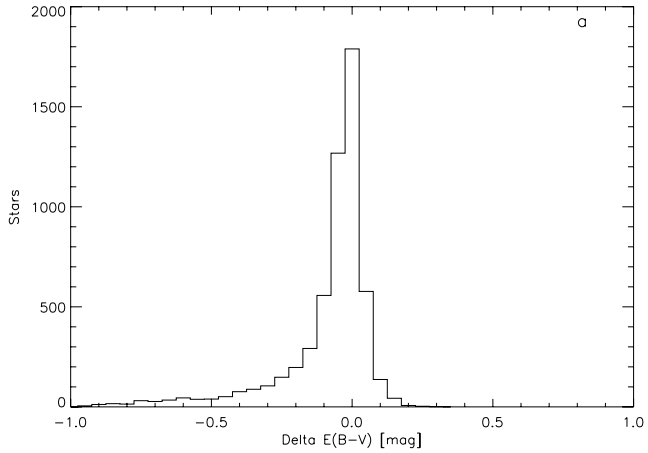

FIG. 12*a*

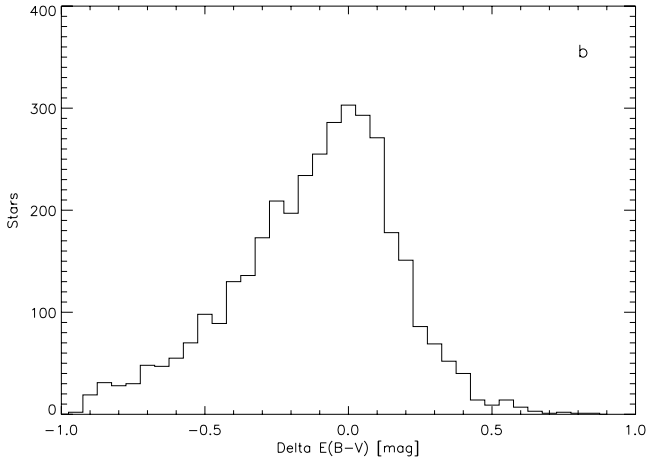

FIG. 12*b*

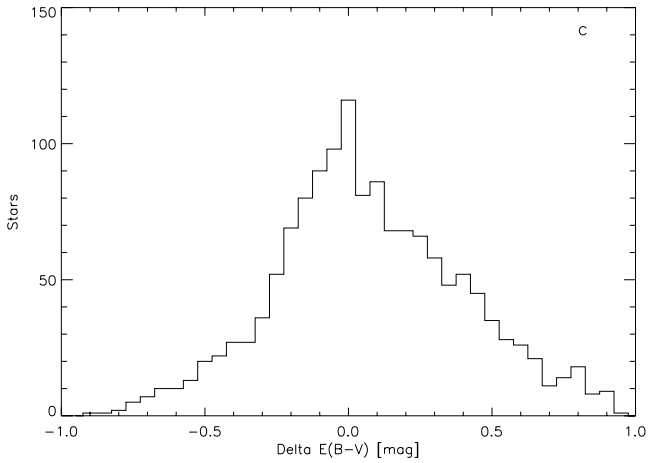

FIG. 12*c*

FIG. 12.—Histograms of errors $\delta E(B-V)$ for stars of the NK80 catalog using model A with the same ranges of distance as in Fig. 11.

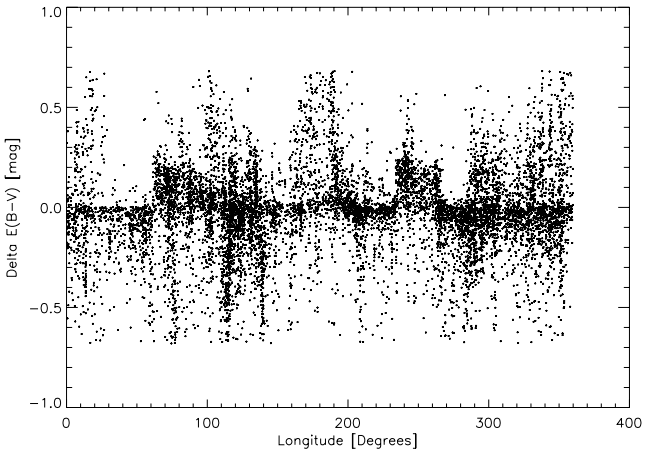

FIG. 13.—Same as Fig. 10 but for model S.

The estimated errors on the distances in the NK80 catalog vary from 15% to 25%, and the errors in A_V are about 0.1–0.2 mag.

In order to further analyze the behavior of the errors as a function of distance, we divided the stars into distance bins of 0.25 kpc. In each bin we obtained the calculated − observed rms $\delta E(B-V)$ of the stars, except when the bin contained less than five stars. Figure 16 shows the variation of the rms with the distance for both models. As expected, the range of distance $d \leq 1.0$ kpc presents the lowest rms. In general, equivalent results are obtained with models A and S.

4.3. *Comparisons with Other Catalogs*

We briefly report here comparisons of our models with two other catalogs. One of the catalogs is that of Guarinos (1992), which contains estimates of extinction and distance of stars derived from *UBV* data and MK types. Most stars are of spectral type O, 4327 in total. Approximately 70% of the stars in the catalog are located at distances less than 0.5 kpc. Half of the stars have $E(B-V)$ up to 0.1 mag. The catalog provides observed and intrinsic $E(B-V)$ for each star. We excluded from our study 2841 stars with $E(B-V)$ equal to 0.

Using model A we calculated the extinction for the stars of the Guarinos (1992) catalog. The rms difference is 0.11, and the correlation coefficient $r = 0.78$; $\delta E(B-V)$ is shown as a function of longitude in Figure 17. The low values of the rms differences can be attributed to the proximity of the stars.

Figure 18 shows the histogram of $\delta E(B-V)$ for the stars of the Guarinos (1992) catalog using model A. We note that approximately 9000 stars have absolute values of $\delta E(B-V)$ smaller than 0.05 mag. For model S the rms was 0.13 mag ($r = 0.75$).

The second catalog discussed in this section is the catalog of ultraviolet interstellar extinction excess for 1415 stars (the Savage catalog; Savage et al. 1985). The data in this catalog were derived from the parameters of extinction of the photometric catalog of 3573 point sources in the UV obtained by the *Astronomical Netherlands Satellite* (Wesselius et al. 1982). The Savage catalog contains normal stars with well-defined spectral characteristics, of spectral type B7 or earlier. The intrinsic errors of $E(B-V)$ are about 0.2 mag, and the errors on distances are about 25%. Low-latitude stars are predominant. The authors of the catalog obtained the distances using Blaauw's (1956) relation of M_V with spectral type and assumed $A_V = 3.1E(B-V)$.

We calculated the extinction for each star of the Savage catalog for both models using values of longitude, latitude, and distance. The rms difference (calculated − observed) obtained for

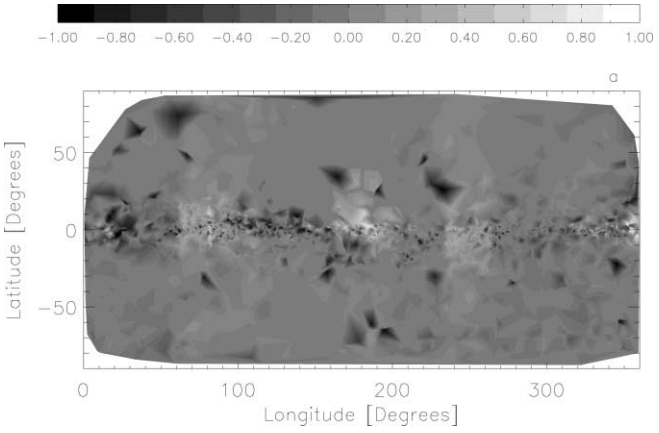

FIG. 14*a*

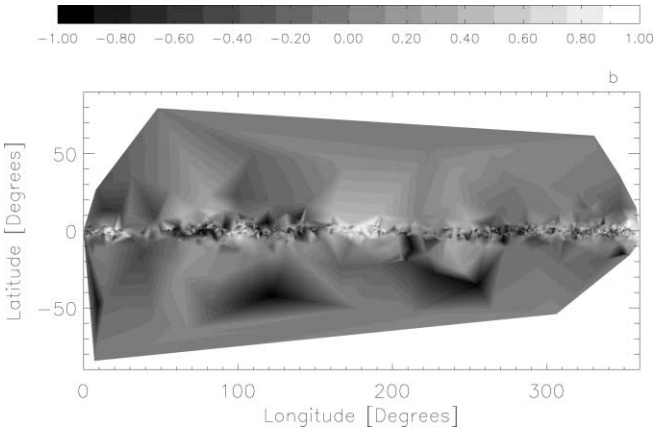

FIG. 14*b*

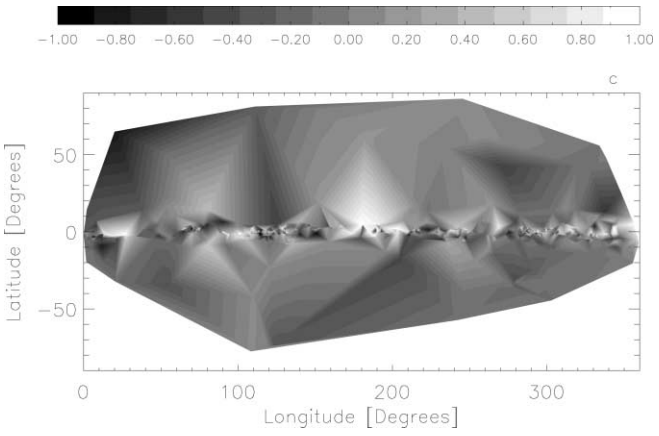

FIG. 14*c*

FIG. 14.—Maps of errors $\delta E(B-V)$ for stars of the NK80 catalog using model S in three ranges of distances d: (*a*) $d \leq 1$ kpc, (*b*) 1.0 kpc $< d \leq 3.0$ kpc, and (*c*) $d > 3.0$ kpc.

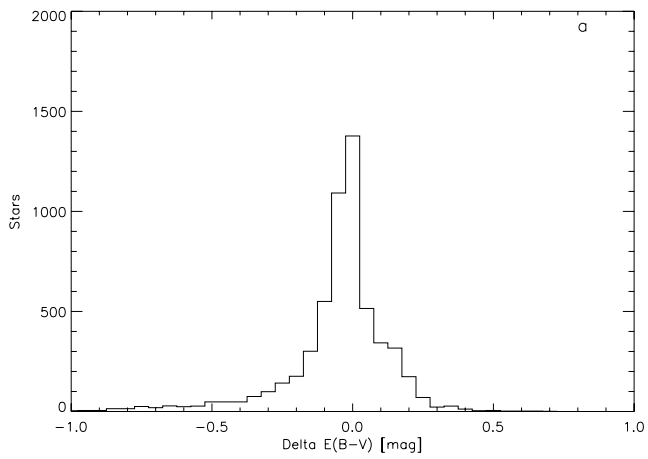

FIG. 15*a*

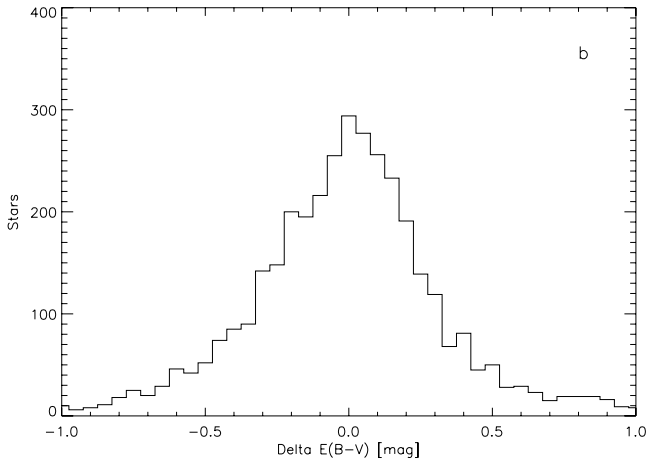

FIG. 15*b*

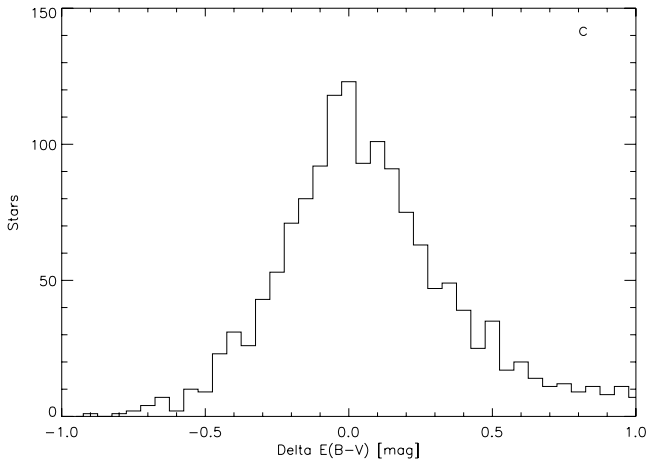

FIG. 15*c*

FIG. 15.—Same as Fig. 12 but for model S.

model S was 0.22, discarding the stars with $\delta E(B-V)$ greater than 3 times the rms. The longitudinal profile of the differences is shown in Figure 19. The correlation coefficient between calculated and observed $E(B-V)$ is $r = 0.77$. We have approximately 1072 stars with absolute values of $\delta E(B-V)$ smaller than 0.15 mag, as shown in Figure 20.

Using model A the rms difference obtained was 0.21 ($r = 0.79$), with approximately 1004 stars with $\delta E(B-V) < 0.15$ mag. These errors are partially due to the intrinsic errors of the catalog, about 25% errors in distances and about 0.20 mag in $E(B-V)$.

Diplas & Savage (1994) published a sample of B2 and hotter stars with interstellar neutral hydrogen column densities obtained from archival Lyα absorption lines observed at high spectral resolution with the *IUE* satellite. The final catalog contains 393 stars with distances ranging from 0.12 to 11 kpc and an average distance of 2.1 kpc. Using model S the rms difference was 0.19, and with model A it was 0.18 ($r = 0.75$).

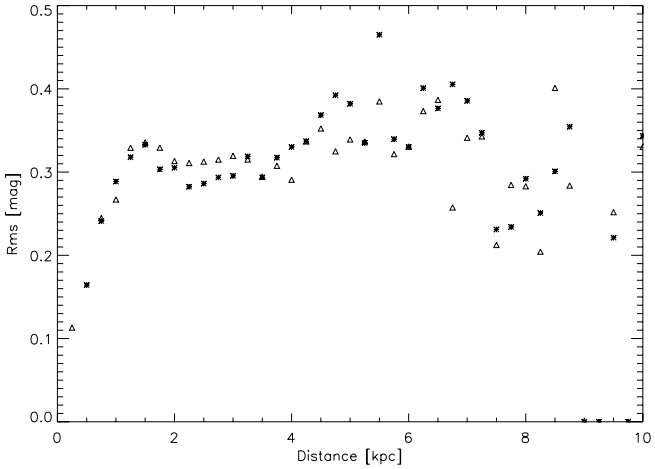

FIG. 16.—The rms as a function of distance for model A (*asterisks*) and model S (*triangles*).

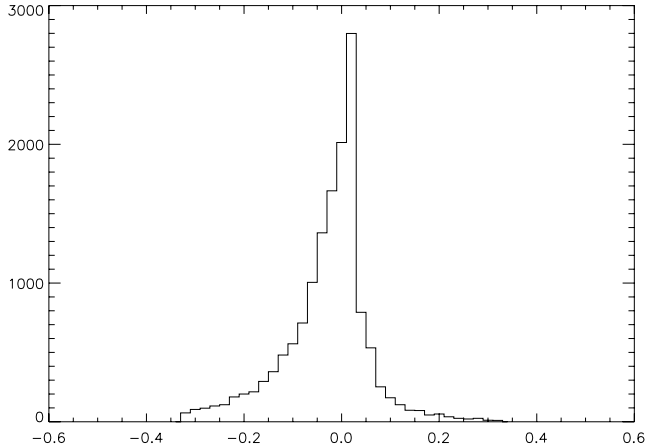

FIG. 18.—Histogram of $\delta E(B-V)$ for stars of the catalog of Guarinos using model A.

4.4. *Corrections Using the $\delta E(B-V)$ of Neighboring Stars*

Any extinction model is subject to errors because of irregularities in the distribution of the interstellar dust. Supposing that the scale sizes of the irregularities are not too small, they may affect neighboring stars in a similar way. It should then be possible to apply local corrections to the model. This can be done by calculating, for a group of neighboring stars, the average difference between model calculations and observations of $E(B-V)$. This difference is then applied as a correction to the object for which we wish to compute the extinction.

We consider as "neighboring stars" those with l and b within a maximum distance $d_{\max}$ of the object studied. In order to test the effectiveness of the correction based on neighboring stars, we first calculated with our models the extinction for the direction and distance of each star of the NK80 catalog and calculated the difference $\delta E(B-V)$, as described in the previous sections. We constructed a new catalog containing these differences. In a second step, for each star we subtracted from its $E(B-V)$ the average $\delta E(B-V)$ of the neighboring stars. The result is the final color excess given by this self-correcting method.

We performed calculations with $d_{\max}$ varying from $0.^{\circ}25$ to 3°. With a too small $d_{\max}$ the number of neighboring stars drops quickly to zero; with a too large $d_{\max}$ the extinction errors of neighboring stars become uncorrelated. The lowest value of the rms errors was obtained for $d_{\max} = 1.^{\circ}25$.

Using this procedure with the axisymmetric model, the rms value of $\delta E(B-V)$ for the NK80 catalog dropped from 0.25 to 0.19 (or smaller, if we rejected points outside 2 σ of the distribution). We found 8512 stars that possessed at least one neighboring star; the final errors are presented as a function of Galactic longitude in Figure 21. When using this correction with model S, the rms $\delta E(B-V)$ dropped from 0.26 to 0.20 mag.

4.5. *Comparison of the Models with DIRBE/IRAS Maps*

The dust maps (SFD98) and programs for reading them are available for download online.[3] We used the map with full resolution (4096×4096 pixels). The grid to compare it with our models for interstellar extinction has a mesh size of 1° in both Galactic longitude and latitude, covering the whole Galaxy.

In this way, there are 64,800 points. For each point we calculated the extinction along the line of sight up to 20 kpc. Using model S the rms difference was 0.27, excluding points with rms greater than 3 σ of the distribution. For model A the rms was 0.26, excluding points with rms greater than 3 σ.

The maps of $\delta E(B-V)$ (calculated − SFD) are shown in Figure 22 for model A (Fig. 22*a*) and model S (Fig. 22*b*). The histograms in Figure 23 show the differences between each of the

[3] See http://astron.berkeley.edu/davis/dust/data/data.html.

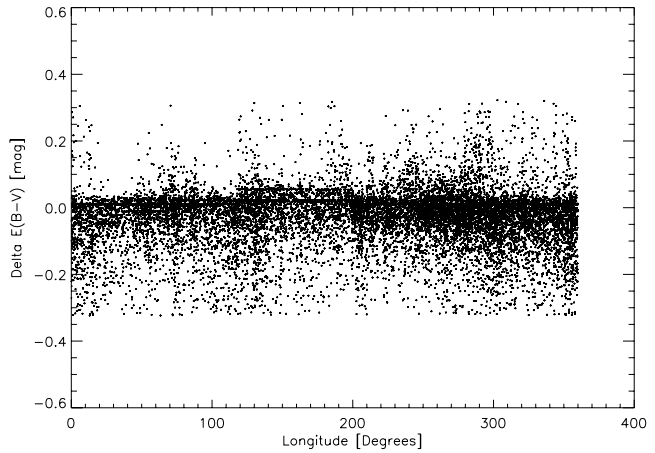

FIG. 17.—Errors $\delta E(B-V)$ as a function of longitude for stars of the catalog of Guarinos using model A.

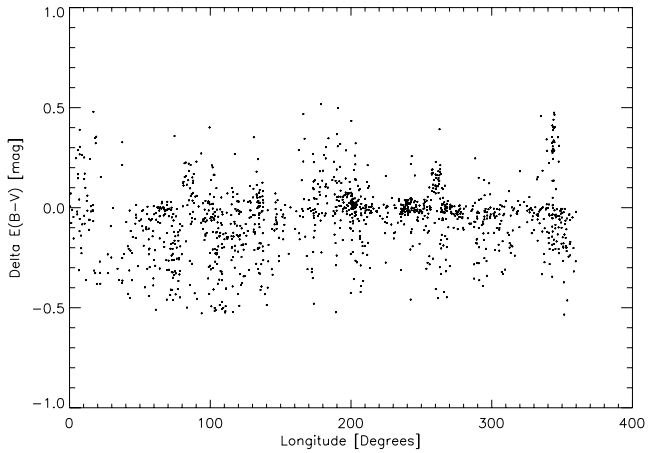

FIG. 19.—Longitudinal profile of errors $\delta E(B-V)$ for stars of the Savage catalog using model S.

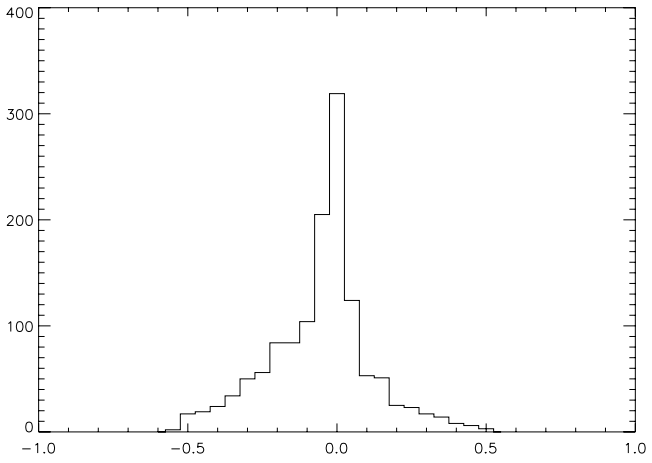

FIG. 20.—Histogram of $\delta E(B-V)$ for stars of the Savage catalog using model S.

models and the DIRBE/*IRAS* extinction map. As can be seen in Figures 22*a* and 22*b*, the largest differences are located in the Galactic plane ($|b| \leq 10^\circ$). In this region we see that $|\delta E(B-V)|$ ranges from -2.10 to 2.10 mag.

The large differences between the rms (calculated − SFD) extinctions in the Galactic plane can be attributed in part to some assumptions made by SFD98: (1) a single temperature for all the dust and (2) dust temperature measured with the 40′ beam of DIRBE. Both approximations are valid at high latitudes but not for large extinction at intermediate and low latitudes, where the molecular gas contributes significantly to the IR emission spectrum and is not well fitted by a single temperature (Reach et al. 1995; Lagache et al. 1998; Chen et al. 1999).

Arce & Goodman (1999, hereafter AG99) studied the interstellar extinction in the Taurus region and compared results obtained using four different techniques and the SFD98 results. The four techniques were (1) using the color excess of background stars for which spectral types are known; (2) using the *IRAS* Sky Survey Atlas 60 and 100 μm images; (3) using star counts; and (4) using an optical (V and R) version of the average color excess used by Lada et al. (1994). The four techniques give basically the same results in terms of A_V values, structure, and extinction, providing a good estimated A_V up to 4 mag. In general, the SFD98 method gives extinctions a factor of 1.3–1.5 larger than the AG99 methods. They concluded that the SFD98 method overestimates the reddening for lines of sights where $A_V > 0.5$ mag.

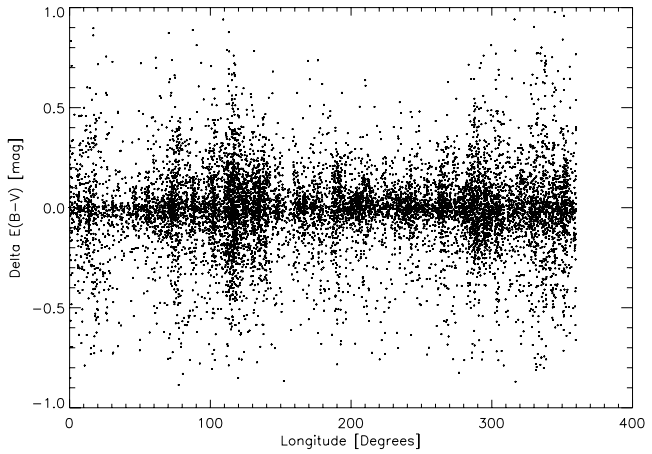

FIG. 21.—Longitudinal profile of $\delta E(B-V)$ for stars of the NK80 catalog compared with model A after corrections for neighboring stars (see text).

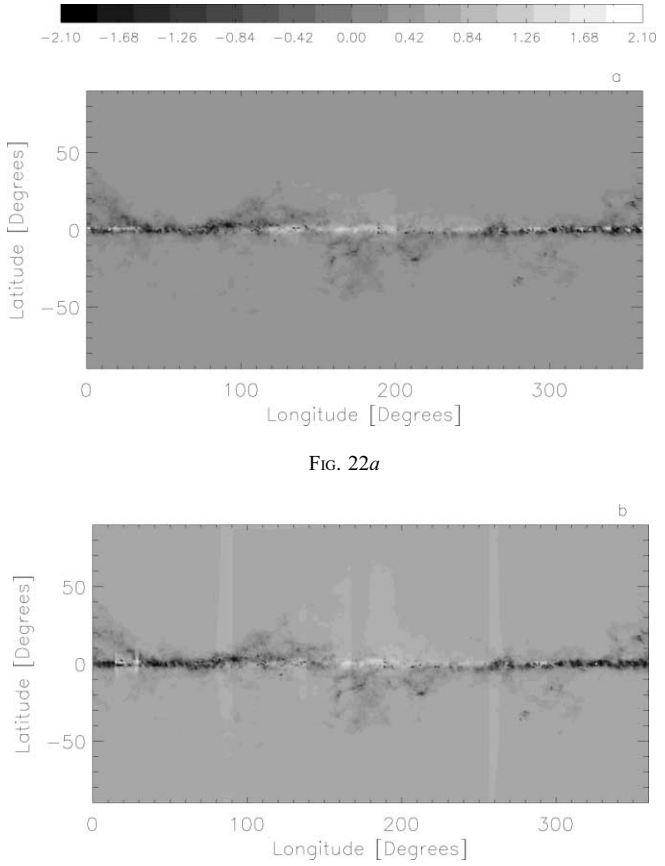

FIG. 22*a*

FIG. 22*b*

FIG. 22.—Maps of differences $\delta E(B-V)$ between SFD98 maps and (*a*) model A and (*b*) model S (see text).

4.6. *Comparison of the Models with the* 100 μm *Brightness*

In § 2 we presented a correction for the observed intensity at 100 μm and showed its correlation with CO, the cold component of the gas. Bloemen et al. (1990) and Sodroski et al. (1987, 1989, 1997) also found correlations between H I, CO, and infrared emission.

As a test for our models, we compared the predictions with the corrected intensity at 100 μm. For this purpose we calculated the integrated extinction along lines of sight in the Galactic disk to distances up to 20 kpc. The calculations were performed at intervals of 1° in l and 0.°5 in b, for absolute Galactic latitudes less than 10° and covering the whole range of longitudes. We compare the calculated $E(B-V)$ from model A and FIR intensity in Figure 24. A good correlation can be observed, which confirms that we can use the gas distribution to estimate the amount of dust along lines of sight in the Galaxy.

4.7. *Comparison of Our Models with Burstein & Heiles Results*

We compared the extinctions predicted by our models along given lines of the sight with those derived from H I/galaxy counts (Burstein & Heiles 1978, 1982). We calculated the integrated extinction (to 20 kpc) using model A, at intervals of 1° in Galactic latitude and longitude for latitudes greater than 10°, in the regions where the values of the Burstein & Heiles (1978, 1982) map are reliable. We excluded from our study the region $230^\circ \leq l \leq 310^\circ$, $-20^\circ \leq b \leq +20^\circ$, where the Burstein & Heiles

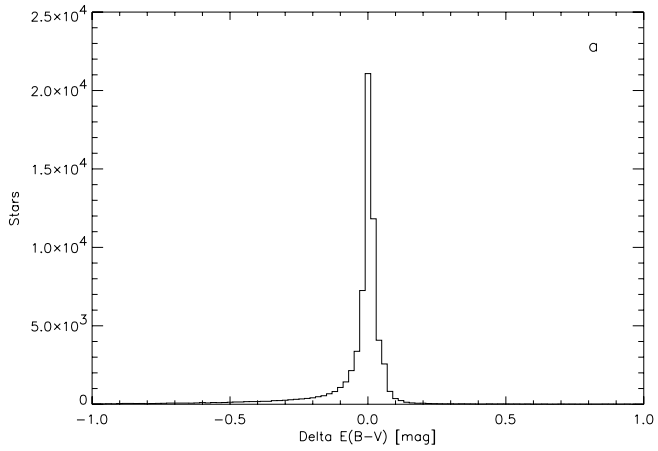

FIG. 23*a*

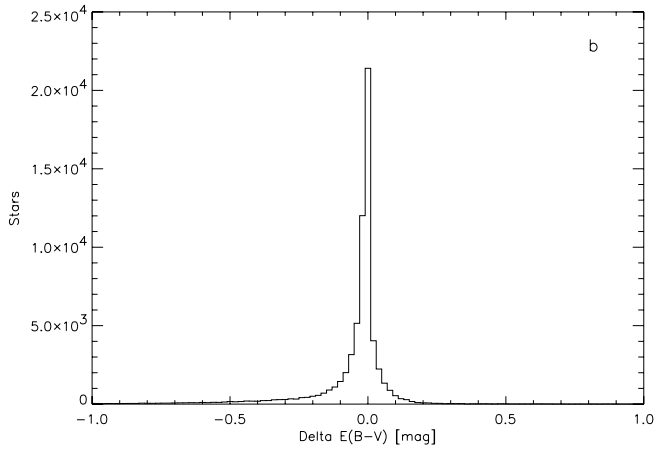

FIG. 23*b*

FIG. 23.—Histograms of the differences $\delta E(B-V)$ from comparisons of our models with SFD98 maps (see text) for (*a*) model A and (*b*) model S.

(1978, 1982) reddening is overestimated (Burstein et al. 1987; Burstein 2003; Hudson 1999).

The rms difference considering both hemispheres was 0.07 mag using model A. In general we find a better correlation at positive latitudes ($r = 0.79$) than at negative ones ($r = 0.76$).

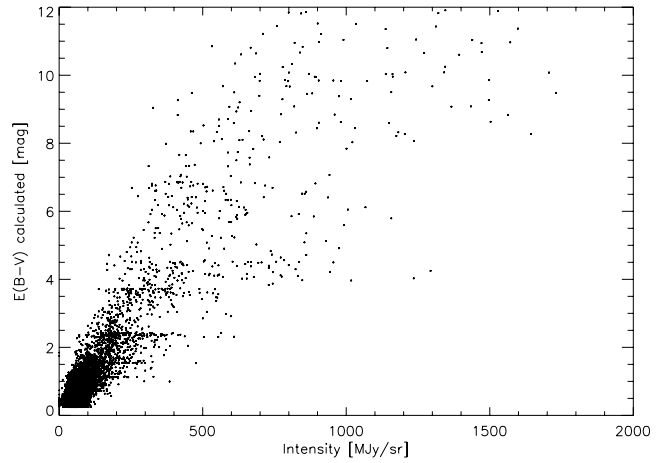

FIG. 24.—Correlation between the extinction calculated using model A and the corrected intensity at 100 μm.

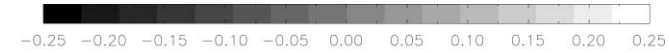

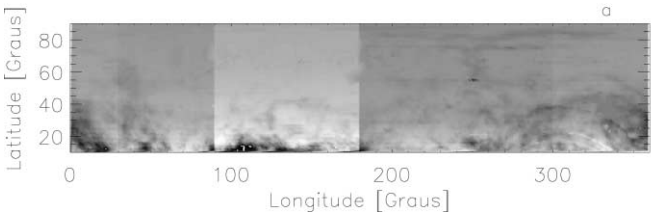

FIG. 25*a*

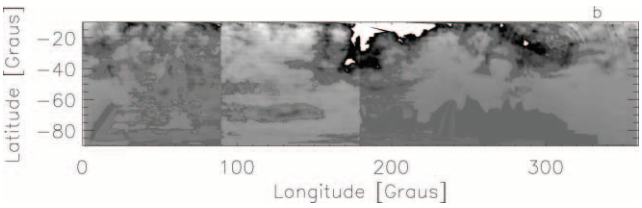

FIG. 25*b*

FIG. 25.—Maps of differences $\delta E(B-V)$ between model A and the Burstein & Heiles (1978, 1982) maps for (*a*) the north Galactic hemisphere and (*b*) the south Galactic hemisphere.

The maps of the differences between model A and the Burstein & Heiles (1978, 1982) predictions are presented in Figure 25. We can see that the largest differences coincide with the regions with molecular cloud complexes. An area that contributes to producing a relatively bad correlation at negative latitudes was found within $160^\circ \leq l \leq 190^\circ$, $-10^\circ \leq b \leq -60^\circ$, as can also be seen in Figure 25*b*. Burstein & Heiles (1982) mentioned this region as presenting a large tongue of reddening, with a low H I gas-to-dust ratio.

5. CONCLUSIONS

We constructed three-dimensional models of the dust distribution in the Galactic disk to estimate the interstellar extinction between the Sun and any point in the Galaxy, given its longitude, latitude, and distance. These models are useful for a large variety of purposes, such as studies of Galactic structure, star count predictions, and extinction corrections for individual objects. We derived the basic parameters of our models from the gas distribution in the Galaxy by fitting with empirical laws the data of neutral hydrogen and CO gas surveys. Examples of these empirical laws are the radial gas density law and the radial variation of the scale height of the gas distribution. One of our models assumes that the gas distribution is axisymmetric (model A), while the other also takes into account the spiral arms (model S).

The calculated extinction values were compared with the observed ones taken from catalogs that contain measured extinctions and distances for large samples of stars. In this way, we were able to specify the probable errors of our method, depending on the distance. Models A and S are equivalent on the average. Since model A is simpler, it may be preferable to use for most purposes. However, model S is certainly useful for detailed studies in nearby regions affected by spiral arms. The main results, concerning probable errors, can be seen in Figures 12 and

15, which present histograms of calculated − observed $E(B-V)$ for three ranges of distances, based on the NK80 catalog of early-type stars. Typically, the standard error for distances between 1 and 3 kpc is on the order of 0.25 mag in $E(B-V)$; for distances larger than 3 kpc the error is about 0.30 mag in $E(B-V)$. These are the probable errors for individual stars, which are largely due to the clumpy nature of the interstellar medium; systematic errors or errors for the average value of the extinction, which are of interest in statistical studies such as star count models of the Galaxy, are much smaller. This can be seen from the fact that the histograms in Figures 12 and 15 are centered on almost zero error.

The column densities derived from our models are well correlated with the infrared emission in the 100 μm band, corrected for effects of dust temperature. This indicates that our basic hypotheses are correct. A relatively good correlation was found with the extinction maps of Burstein & Heiles (1978, 1982), which were derived in part from galaxy counts. However, our results are more reliable, since they produce better correlation with other extinction indicators. We also compared our models with SFD98 maps, which present systematic errors that were already pointed out in the literature and are confirmed here. Note that $E(B-V)$ from SFD98 maps is on average 1.20 times larger than $E(B-V)$ obtained with our models, in agreement with the factor obtained by Chen et al. (1999).

The self-correcting procedure, which introduces corrections to our models based on the neighboring stars of an object to be studied, is not useful for Galactic structure studies but is able to decrease the probable error for the extinction of individual objects. For instance, using the stars of the NK80 catalog for corrections, rms errors for $E(B-V)$ as low as 0.19 can be reached. We recall that the observational errors for $E(B-V)$ in the NK80 catalog are on the order of 0.05 mag, so that the intrinsic errors of the models are smaller than those mentioned above. However, the errors are probably larger for the inner parts of the Galaxy ($R < 2$ kpc), since the extinction is large and the available catalogs do not contain enough stars in that region to validate the models.

Our models will be available online[4] or can be obtained on request from one of the authors.

Financial support for this work was provided by the Conselho Nacional para o Desenvolvimento Científico e Tecnológico (CNPq), Coordenacão de Aperfeiçoamento Pessoal de Nível Superior, the Núcleo de Excelência em Galáxias, and the Instituto do Milênio para Evolução de Estrelas e Galáxias na Era Dos Grandes Telescópios. E. A. has CNPq fellowships 141733/2000-4 and 2003/201113-3. We also thank the anonymous referee for useful comments on the manuscript.

[4] See http://www.astro.iag.usp.br/~amores.

REFERENCES

Amôres, E. B. 2000, M.S. thesis, Univ. São Paulo
Arce, H. G., & Goodman, A. A. 1999, ApJ, 512, L135 (AG99)
Arenou, F., Grenon, M., & Gómez, A. 1992, A&A, 258, 104
Babu, G. J., & Feigelson, E. D. 1996, Astrostatistics (New York: Chapman & Hall)
Blaauw, A. 1956, ApJ, 123, 408
Bloemen, J. B. G. M., Deul, E. R., & Thaddeus, P. 1990, A&A, 233, 437
Bohlin, R. C., Savage, B. D., & Drake, J. F. 1978, ApJ, 224, 132
Boulanger, F., Bronfman, L., Dame, T. M., & Thaddeus, P. 1998, A&A, 332, 273
Bronfman, L., Casassus, S., May, J., & Nyman, L.-A. 2000, A&A, 358, 521
Burstein, D. 2003, AJ, 126, 1849
Burstein, D., & Heiles, C. 1978, ApJ, 225, 40
———. 1982, AJ, 87, 1165
Burstein, D., Krumm, N., & Salpeter, E. E. 1987, AJ, 94, 883
Burton, W. B., & Liszt, H. S. 1983, A&AS, 52, 63 (BL83)
Chen, B., Figueras, F., Torra, J., Jordi, C., Luri, X., & Galadí-Enríquez, D. 1999, A&A, 352, 459
Cox, P., & Mezger, P. G. 1989, A&A Rev., 1, 49
Dame, T. M., Ungerechts, T. M., Cohen, R. S., & Thaddeus, P. 2001, ApJ, 547, 792
Dame, T. M., et al. 1987, ApJ, 322, 706
Diplas, A., & Savage, B. 1994, ApJ, 427, 274
Englmaier, P., & Gerhard, O. 1999, MNRAS, 304, 512
Fitzgerald, M. P. 1968, AJ, 73, 983
Guarinos, J. 1992, Ph.D. thesis, Strasbourg Obs.
Guibert, J., Lequeux, J., & Viallefond, F. 1978, A&A, 68, 1
Hakkila, J., Myers, J., & Stidham, B. 1997, AJ, 114, 2043
Hammersley, P. L., Garzón F., Mahoney, T., & Calbet, X. 1995, MNRAS, 273, 206
Hauser, M., et al. 1984, ApJ, 285, 74
Hudson, M. 1999, in ASP Conf. Ser. 111, Magnetic Reconnection in the Solar Atmosphere, ed. R. D. Bentley & J. T. Mariska (San Francisco: ASP), 57
Kerr, F. J., Bowers, P. F., Jackson, P. D., & Kerr, M. 1986, A&AS, 66, 373
Kim, S., & Martin, P. G. 1996, ApJ, 462, 296
Lada, C. J., Lada, E. A., Clemens, D. P., & Bally, J. 1994, ApJ, 429, 694
Lagache, G., Abergel, A., Boulanger, F., & Puget, J. L. 1998, A&A, 333, 709
Laureijs, R. J., Clark, F. O., & Prusti, T. 1991, ApJ, 372, 185
Lee, H. M., & Draine, B. T. 1985, ApJ, 290, 211
Lépine, J. R. D., Mishurov, Yu. N., & Dedikov, S. Yu. 2001, ApJ, 546, 234
Lucke, P. B. 1978, A&A, 64, 367
Marinho, E. P., & Lépine, J. R. D. 2000, A&AS, 142, 165
Méndez, R. A., & van Altena, W. F. 1998, A&A, 330, 910 (MvA98)
Neckel, T., & Klare, G. 1980, A&AS, 42, 251 (NK80)
Parenago, P. P. 1940, AZh, 17, 3
Perry, C. L., & Johnston, L. 1982, ApJS, 50, 451
Reach, W. T., et al. 1995, ApJ, 451, 188
Reid, M. J. 1993, ARA&A, 31, 345
Russeil, D. 2003, A&A, 397, 133
Sanders, D. B., Solomon, P. M., & Scoville, N. Z. 1984, ApJ, 276, 182
Savage, B. D., Massa, D., & Meade, M. 1985, ApJS, 59, 397
Schlegel, D. J., Finkbeiner, D. P., & Davis, M. 1998, ApJ, 500, 525 (SFD98)
Sodroski, T. J., Dwek, E., Hauser, M. G., & Kerr, F. J. 1987, ApJ, 322, 101
———. 1989, ApJ, 336, 762
Sodroski, T. J., Odegard, N., Arendt, R. G., Dwek, E., Weiland, J. L., Hauser, M. G., & Kelsall, T. 1997, ApJ, 480, 173
Terebey S., & Fich, M. 1986, ApJ, 309, L73
Trumpler, R. J. 1930, Lick Obs. Bull., 14, 154
Vallée, J. P. 2002, ApJ, 566, 261
Weaver, H., & Williams, D. R. W. 1973, A&AS, 8, 1
Wesselius, P. R., van Duinen, R. J., de Jonge, A. R. W., Aalders, J. W. G., Luinge, W., & Wildeman, K. J. 1982, A&AS, 49, 427
Whittet, D. C. B. 1992, Dust in the Galactic Environment (Bristol: IOP)
Xu, C., Buat, V., Boselli, A., & Gavazzi, G. 1997, A&A, 324, 32